SCIENCE CHINA
Physics, Mechanics & Astronomy

• Article •
Special Topic: Airworthiness and Fatigue

January 2014 Vol.57 No.1: 74–82
doi: 10.1007/s11433-013-5332-x

Effects of loading condition on very-high-cycle fatigue behaviour and dominant variable analysis

LEI ZhengQiang[1,2], XIE JiJia[1], SUN ChengQi[1] & HONG YouShi[1*]

[1] *State Key Laboratory of Nonlinear Mechanics, Institute of Mechanics, Chinese Academy of Sciences, Beijing 100190, China;*
[2] *PetroChina Pipeline R&D Center, Langfang 065000, China*

Received May 11, 2013; accepted September 27, 2013; published online December 10, 2013

The specimens of a high carbon chromium steel were quenched and tempered at 150°C, 180°C and 300°C. Such specimens were tested via rotating bending and a push-pull type of axial loading to investigate the influences of loading condition on the behaviour of very-high-cycle fatigue (VHCF). Experimental results show the different influences of inclusion size on the fatigue life for the two loading conditions. Predominant factors and mechanism for the fine-granular-area (FGA) of crack origin were discussed. In addition, a reliability analysis based on a modified Tanaka-Mura model was carried out to evaluate the sensitivity of inclusion size, stress, and ΔK_{FGA} to the life of VHCF crack initiation.

very-high-cycle fatigue, FGA, loading condition, life scatter, inclusion

PACS number(s): 46.50.+a, 62.20.Mk, 61.72.Qq

Citation: Lei Z Q, Xie J J, Sun C Q, et al. Effects of loading condition on very-high-cycle fatigue behaviour and dominant variable analysis. Sci China-Phys Mech Astron, 2014, 57: 74–82, doi: 10.1007/s11433-013-5332-x

1 Introduction

Very-high-cycle fatigue (VHCF) is the fatigue failure of metallic materials with the number of loading cycles beyond 10^7. There is an increasing demand of interpretation for the behaviour and mechanism of VHCF crack initiation and life scatter, due to the safety design for industrial structures or components, especially for aircrafts, automobiles, ships, and railways, which need to endure a long period of cyclic loading up to 10^{10} cycles. Naito et al. [1] indicated that VHCF has its particular features for high strength steels and started systematic study for this topic in 1980s. S-N curves for high strength steels including VHCF regime often present a step-wise tendency (duplex S-N curves [2]), and it is a challenge for the safety design of industrial structures or components under the current criterion of conventional fatigue limit defined at 10^7 loading cycles. The behaviour of VHCF fatigue crack initiation and propagation may become comparably significant for airworthiness.

The influence of loading condition, namely the control volume and loading frequency, on VHCF has been studied, in which the concept of control volume was first proposed by Murakami et al. [3] to interpret the decrease of fatigue strength under axial loading. Control volume is defined as the volume of the tested part of the specimen, in which potential fracture origins exist. The control volume for axial loading specimens is about several times of that for rotating bending specimens because of the existence of stress gradient for the latter condition. The inclusion size under axial cycling is with distribution potentially larger than that under rotating bending; thus the fatigue strength is degraded under axial loading [4]. Loading frequency may influence the fatigue strength of materials, and its effects differ with different microstructures. Zhao et al. [5] revealed that loading frequency has little influence on specimens with higher tensile strength, whereas for the other specimens with lower

*Corresponding author (email: hongys@imech.ac.cn)

tensile strength the fatigue resistance is markedly high in ultrasonic cyclic testing. Zhang et al. [6] found that the higher frequency produced an upper shift of the S-N curves for superalloy IN718. Tschegg et al. [7] indicated that the fatigue strength of bcc metals is more sensitive to loading frequency. However, loading frequency does not change the failure mode of specimens [8].

For VHCF, loading stress is always below the conventional fatigue limit, and the interior defects such as non-metallic inclusions acting as a stress raiser become fatigue crack origin with the pattern of fine-granular-area (FGA) [9] on fracture surface. Recent studies [10,11] have confirmed the existence of fine grains in FGA. Surface defects may become non-propagating cracks [12], and sometimes grain boundary could also become a crack origin for high carbon chromium steel under low tempering temperature [5,13]. It is also revealed that fatigue crack initiation within FGA is dominated for high cycle fatigue (HCF) and VHCF, and FGA consumes more than 90% fatigue life [14,15]. Thus, microstructure barriers near the fatigue crack origin are responsible for crack initiation and determine the fatigue life scattering. On the contrary, fatigue cracks grow in elastic-plastic field with less microstructural influence for low cycle fatigue (LCF) [16]. Studies on VHCF mechanism have shown that it is the microstructure that plays an important role in the process of interior fatigue crack initiation with FGA morphology. The predominant features of microstructure include spherical carbide [17], hydrogen [18], inclusion size [19], and chemical compositions of inclusion [20]. It is also reported that, the threshold value of VHCF crack initiation ΔK_{FGA} is approximately equal to the threshold value of crack propagation ΔK_{th} regardless of the microstructures [21].

The location of dominated inclusion either near the surface or far from the surface is the key factor to the failure mode transition with or without FGA, and leads to the large scatter of S-N curves [16,22]. A number of studies on fatigue crack propagation also show that fatigue crack growth behaviour near the threshold differs with respect to the change of tempering temperature [23–25].

In this paper, a type of high strength steel was used and the specimens were quenched and then tempered at 150°C, 180°C and 300°C, respectively. Rotating bending and axial loading fatigue tests were performed to investigate the influence of loading condition on the S-N curve scatter from the LCF regime to the VHCF regime. And the reliability analysis based on a modified Tanaka-Mura model was carried out to evaluate the sensitivity of inclusion size, stress, and ΔK_{FGA} for the fatigue failure with interior inclusion initiation.

2 Experimental procedure

The test material is a high carbon chromium steel with the chemical compositions (wt.%) of: 1.06 C, 1.04 Cr, 0.88 Mn, 0.34 Si, 0.027 P and 0.005 S (Fe balance). The specimens were austenitized at 845°C for 2 hours in a vacuum, then oil-quenched and tempered for 2 hours in a vacuum at 150°C, 180°C and 300°C, respectively. Such heat-treated specimens are of the microstructure with tempered martensite, retained austenite and carbides. The volume fractions of retained austenite decrease as tempering temperature increases from 150°C, 180°C, to 300°C , which was measured by means of X-ray diffraction (tube: Cu-K_{α}, voltage: 40kV, current: 40 mA, scanning speed: 1°/min) with the results shown in Figure 1. With respect to the heat treatment procedure and the loading condition, the specimens are classified into six groups, the code and mechanical properties of each specimen group are listed in Table 1.

Rotating bending fatigue test was performed for RB specimen groups by using a “Giga-Quad” machine at room temperature with the rotating speed of 3150 rpm (frequency 52.5 Hz) and the stress ratio of −1. Push-pull type of axial cycling was performed for “UL” specimens by a Shimadzu USF-2000 ultrasonic machine at a resonance frequency of 20 kHz at room temperature, also with the stress ratio of −1. The geometries of two types of specimens are shown in Figure 2. The round notch surface was ground by grade 400, 800, 1500 and 2000 abrasive papers and polished to a smooth finish.

3 Experimental results

Figure 3(a) shows the S-N data for the three groups of specimens under rotating bending fatigue test. It is seen that the shape of the S-N curves differs from each other for the three types of heat treatment with the same material. For RB150, the S-N data almost display a tendency of straight line. The shape of S-N data of RB180 presents a duplex or

Table 1 Mechanical properties of six groups of specimens

Specimen group		Tempering temp (°C)	Micro-hardness Hv (kgf/mm^2)[a)]	Tensile stress σ_b (MPa)
Rotating bending	Axial loading			
RB150	UL150	150	808	2163
RB180	UL180	180	753	1849
RB300	UL300	300	666	1690

a) Load is 100 gf with holding time of 15 s.

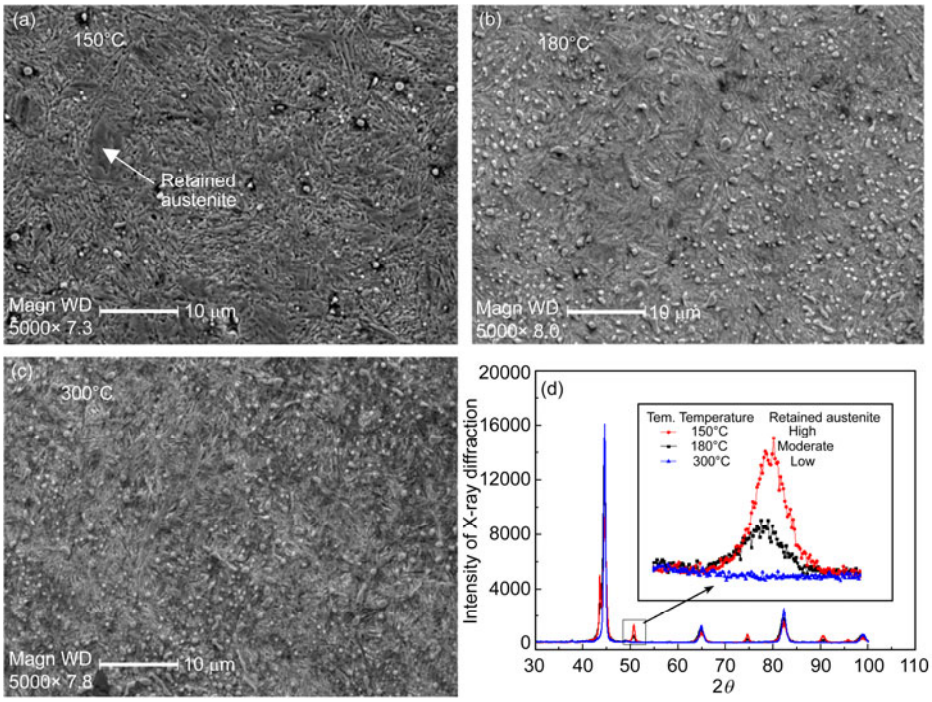

Figure 1 (Color online) Micrographs of acid-etched surfaces for specimens tempered at (a) 150°C, (b) 180°C and (c) 300°C, and (d) results of X-ray diffraction measurements for retained austenite content.

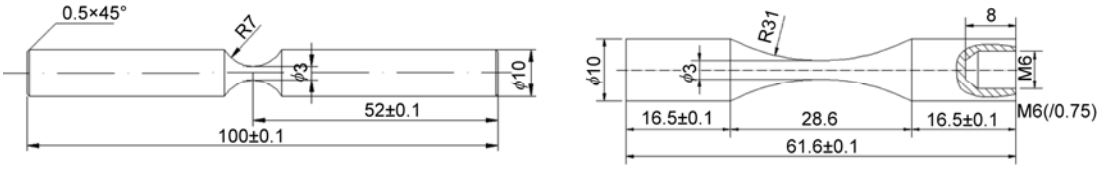

Figure 2 Specimens for fatigue tests: (a) for rotating bending test and (b) for ultrasonic cyclic test.

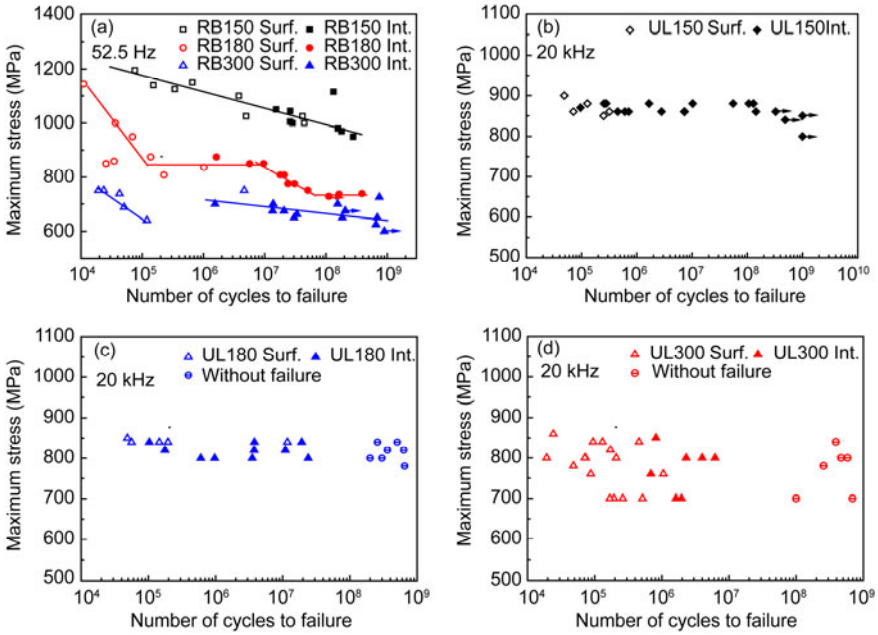

Figure 3 (Color online) S-N data of 150°C, 180°C and 300°C tempered specimens under rotating bending loading and ultrasonic cycling. (Surf.: surface initiation, Int.: interior initiation).

stepwise tendency which is one of the VHCF specific characteristics for high strength steels [2]. The S-N data scattered around two separated lines for RB300, resulting in the uncertainty of fatigue life at a given stress level. For example, fatigue failures occurred at 10^4, 10^6, 10^7, or 10^8 cycles when the maximum stress was about 700 MPa. The changes of the shape of S-N curves lead to a large life scattering for the three groups of specimens. The comparison of these three groups of S-N data shows an increasing tendency of life scatter as the tempering temperature changes from 150°C to 300°C.

Similar scattering properties are also seen in axial loading fatigue tests. Figures 3(b)–3(d) are the S-N data for UL150, UL180 and UL300 respectively. For UL150 specimens subjected to axial cycling at almost the same level of the maximum stress (860–880 MPa), the results of fatigue life show a very large scattering. The difference of the fatigue life is as large as three orders of magnitude, ranging from 10^5 to 10^8 for crack initiation from interior inclusion. For UL180, the maximum stress ranges between 800–840 MPa, and some specimens run out after 1×10^8 cycles. For UL300, the maximum stress ranges between 780–860 MPa, and most fatigue failure originates from surface defects, with both the fatigue life and strength presenting significantly scattering.

Figure 4 shows the typical morphology of fracture surface for crack interior initiation. For rotating bending, fatigue crack tends to originate from the subsurface of specimen, and the fisheye pattern is always tangent to the specimen surface (Figure 4(a)), whereas fatigue crack origin is more close to the centre of the cross section for axial cycling (Figure 4(b)). Interior defects include non-inclusion inhomogeneities and equiaxed inclusions. The non-inclusion inhomogeneities are grain boundaries and large clusters as shown in Figures 4(c) and 4(d). Sometimes FGA due to non- inclusion initiation is observed as Figure 4(d) shows. In most cases, VHCF crack initiates from interior inclusion with FGA as shown in Figure 4(e). With the observation on fracture surface by atomic force microscopy (AFM), FGA is composed of fine grains of 300–700 nm in size (Figure 4(f)).

The values of stress intensity factor range at the periphery of inclusion (ΔK_{Inc}), FGA (ΔK_{FGA}) and fisheye ($\Delta K_{\mathrm{fisheye}}$) are calculated by using the following equation [26]:

$$\Delta K = 0.5\sigma_{\mathrm{local}}\sqrt{\pi\sqrt{\mathrm{area}}}, \tag{1}$$

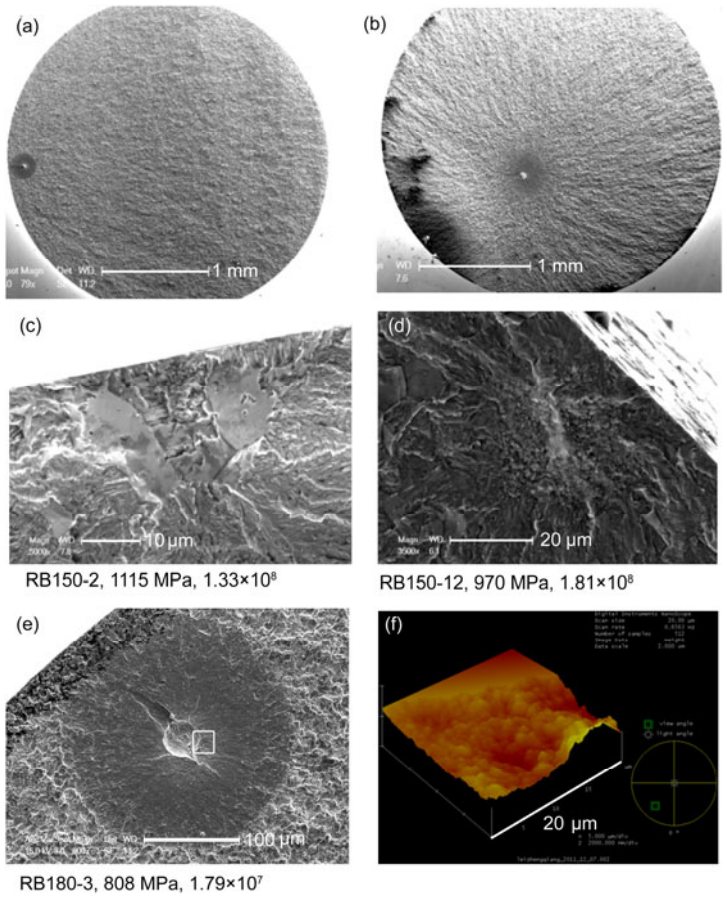

Figure 4 (Color online) Typical morphology of fracture surface. (a) Interior inclusion initiation for rotating bending, (b) interior inclusion initiation for axial cycling, (c) interior grains boundary initiation for RB150, (d) interior non-inclusion initiation with FGA for RB150, (e) fisheye pattern with FGA for VHCF, and (f) AFM observations of FGA in the area marked in (e).

where σ_{local} is the local stress and $\sqrt{area}$ is the equivalent size of inclusion, FGA or fisheye. For the specimens having experienced the rotating bending test, the local stress was calculated as:

$$\sigma_{local} = \left(1 - \frac{d_{Inc}}{R}\right)\sigma_{max}, \quad (2)$$

where R is the radius of the cross section, d_{Inc} is the depth of the inclusion defined as the distance between the inclusion and the nearest surface of specimen, and σ_{max} is the maximum stress at specimen surface. The calculated values of ΔK_{Inc}, ΔK_{FGA} and $\Delta K_{fisheye}$ are shown in Figure 5, in which most data of ΔK_{FGA} are between 5 and 6 MPa $m^{1/2}$. The values of ΔK_{Inc} are below that of ΔK_{FGA}, displaying a slightly decreasing trend with respect to fatigue life. The values of $\Delta K_{fisheye}$ range from 5 to 12 MPa $m^{1/2}$ for rotating bending, whereas the values are slightly higher for axial cycling with the range between 7 and 15 MPa $m^{1/2}$.

The behaviour of interior crack initiation is affected by the microstructure and loading condition. Table 2 lists the statistical results of fatigue crack initiation for all the specimens with the two loading conditions. The fraction of interior inclusion initiation is changed due to different heat treatment procedures and loading condition. For rotating bending, most of interior defects are the types of non-inclusions; only one specimen fractures from interior inclusion for RB150. With the increase of tempering temperature, inclusion initiation becomes dominant for RB150 and RB180 as are often reported in the literature [5,15,22,27–29]. ΔK_{Inc} and ΔK_{FGA} are different from each other for the three heat treatment procedures. For axial cycling, all the specimens are with interior crack initiation originating from inclusions.

4 Effects of loading condition on fatigue crack initiation

The control volume is an important factor influencing fatigue behaviour, which depends on loading condition, as shown in Figure 6. Control volume is defined as a potential volume of fatigue crack origin, for which stress condition is met as $\sigma > \gamma\sigma_0$, where σ_0 is the maximum stress at the specimen surface [4]. The value of γ is assumed to be 0.9 in this study. For a funnel-like specimen, as shown in Figure 2, the radius of curved surface is R, and the minimum diameter of the cross-section is d. Hence the control volume can be calculated with eq. (3). The values of control volume are 5.06 mm^3 and 33.26 mm^3 for rotating bending and axial cycling respectively. For the larger control volume of axial cycling, fatigue crack is more prone to originate at larger inclusion.

For rotating bending:

$$d_1 = d/\sqrt[3]{\gamma},\ z_1 = \sqrt{R^2 - \left[R - 0.5\left(d - d_1\right)\right]^2},$$
$$V \approx 0.5\pi\left(1-\gamma\right)\left(d + d_1\right)^2 z_1,$$

For axial cycling:

$$d_1 = d/\sqrt{\gamma},\ z_1 = \sqrt{R^2 - \left[R - 0.5\left(d - d_1\right)\right]^2},$$
$$V \approx \pi\left(d^2 + d_1^2 + d \cdot d_1\right) z_1 / 6. \quad (3)$$

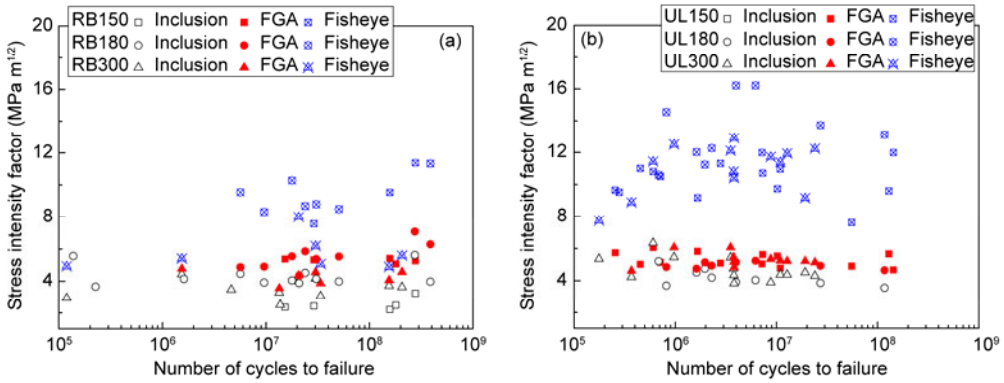

Figure 5 (Color online) ΔK of FGA, inclusion and fisheye *vs* number of cycles to failure: (a) rotating bending and (b) axial cycling.

Table 2 Statistical results of fatigue crack initiation for two loading conditions

	Fraction of interior inclusion initiation	ΔK_{FGA} (MPa $m^{1/2}$)		ΔK_{Inc} (MPa $m^{1/2}$)	
		Mean value	Standard deviation	Mean value	Standard deviation
RB150	11% (1/9)[a)]	5.29	0.10	2.54	0.28
RB180	100% (9/9)[a)]	5.52	0.58	4.27	0.39
RB300	73% (8/11)[a)]	4.31	0.36	3.83	0.51
UL150		5.31	0.45	4.77	0.81
UL180	100%	5.33	0.49	4.71	0.73
UL300		4.93	0.21	4.19	0.54

a) Number of specimens

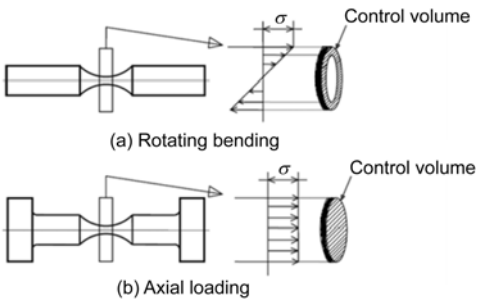

Figure 6 Schematic illustration of the control volume depending on the loading condition [4].

Under rotating bending, fisheye is always tangent to the specimen surface and the fatigue crack origin is located within hundreds of microns for d_{Inc} as shown in Figure 7(a). For axial cycling, the maximum value of d_{Inc} reaches 1.4 mm (Figure 7(b)), which is close to the centre of the specimen. By the comparison of fisheye size to d_{Inc} for the two loading conditions in Figure 7, it is clearly seen that the formation of fisheye and the initiation site are dependent on the inclusion location (d_{Inc}) under rotating bending due to the smaller control volume.

Furthermore, the size of the inclusion as crack origin is also related to the control volume. As shown in Figure 8, the distribution of inclusion size under axial cycling is in larger size than that under rotating bending. The distribution of the inclusions as crack origin presents an obvious peak at the sizes of 30–40 μm under rotating bending, whereas the

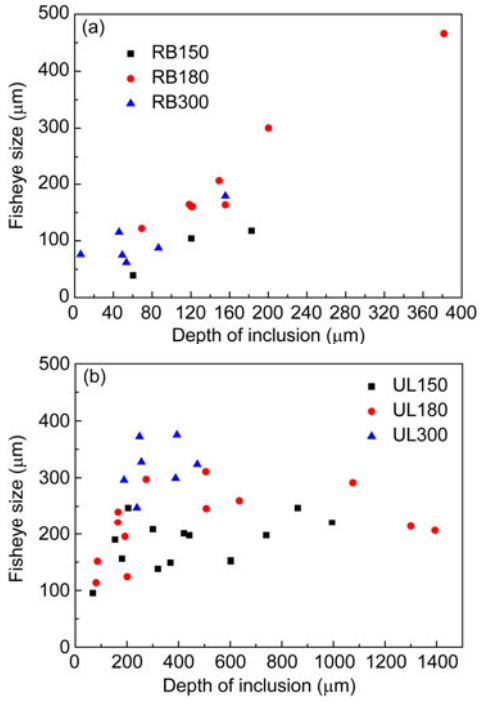

Figure 7 (Color online) Relationship between the fisheye size and the inclusion location: (a) rotating bending and (b) axial cycling.

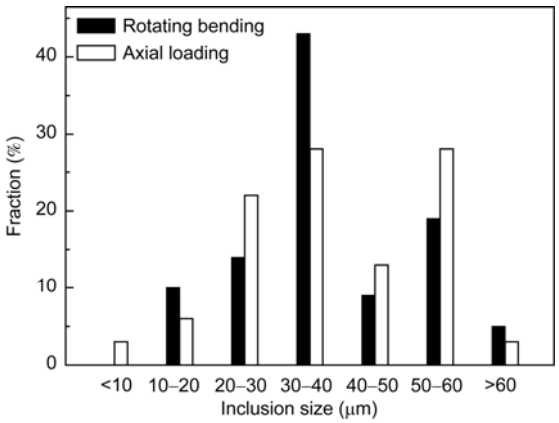

Figure 8 Influence of loading condition on the size of inclusion at crack origin.

distribution of most such inclusions is in the range of 20–60 μm under axial cycling. However, the average size of such inclusions is about 40 μm for both rotating bending and axial cycling. Therefore, the state of larger control volume results in a wider distribution of size of inclusions which are responsible for crack initiation. Similar results were also reported with respect to the effects of loading condition on the size of inclusion as crack origin by Nakajima et al. [4].

Fatigue life is certainly related to the inclusion as fracture origin. As for the S-N data of UL150 mentioned above, there is a large scattering of fatigue life at the same stress level, and the fatigue life increases with the decrease of the inclusion size as shown in Figure 9(b). Figure 9(a) shows the relationship between the inclusion size and the fatigue life for rotating bending; fatigue life seems to be independent of inclusion size, although the applied stress varies for these points as shown in Figure 3(a). However for axial cycling, an obvious increasing tendency of fatigue life is found when inclusion size decreases (Figure 9(b)), for which the datum points are within a small range of applied stress (Figure 3(b)).

5 Dominant variable sensitivity analysis

The distinct difference between rotating bending and axial cycling is the stress distribution in the cross section. This difference produces the variation of local stress at crack initiation site, resulting in the different distribution characteristics of the size of inclusion as crack origin and the scattering of fatigue life for relevant S-N data. Generally, fatigue life is determined by the factors of inclusion size, local stress, tensile strength, etc. And the sensitivity to fatigue failure of a certain variable can be evaluated by the method of variable sensitivity analysis.

A couple of statements have been made regarding the FGA formation: (1) FGA is accompanied by VHCF crack initiation from interior inclusion for high carbon steels [29],

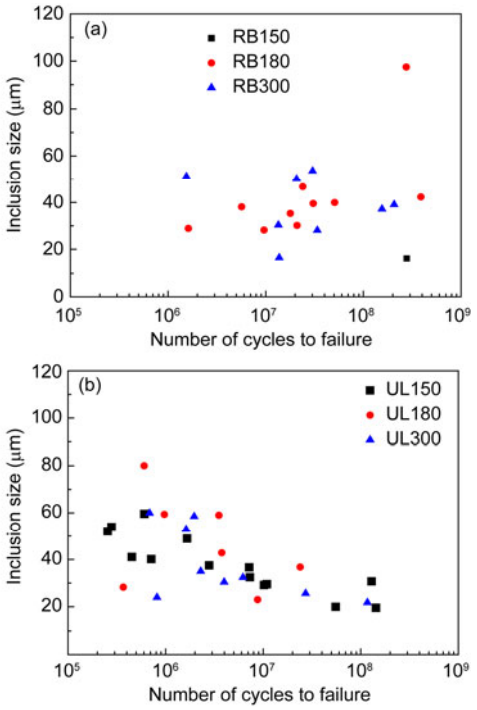

Figure 9 (Color online) Relationship between the inclusion size and the fatigue life: (a) rotating bending and (b) axial cycling.

(2) FGA consumes more than 90 percent of VHCF life [12,14,17], and (3) FGA is finished when the plastic zone size of the microcrack exceeds the width of the martensite [21]. Here, we further assume that dislocations are piled up along the slip band in the martensite as described by the Tanaka-Mura model [30,31], and take into account the influence of tensile strength and FGA size on VHCF crack initiation life. Thus we have the modified Tanaka-Mura model for the life prediction of FGA [32]:

$$N_{\mathrm{FGA}}\pi\left(\tau-\kappa\right)^{2} l_{\mathrm{m}}{}^{2} / G=C\sigma_{\mathrm{b}}\left(\mathrm{area}_{\mathrm{FGA}}-\mathrm{area}_{\mathrm{Inc}}\right), \tag{4}$$

where l_{m} is the width of martensite, σ_{b} is tensile strength of the material, G is bulk shear modulus and C is a correction coefficient reflecting the relation between the strength of martensite and the tensile strength of material. Other parameters are the same as those in the Tanaka-Mura model [30]. With von Mises yield criteria, eq. (4) can be expressed as:

$$N_{\mathrm{FGA}}=\frac{9CG\sigma_{\mathrm{b}}}{2\pi l_{\mathrm{m}}{}^{2}\left(\sigma\text{-}\sigma_{\mathrm{D}}\right)^{2}}\left(\frac{16\Delta K_{\mathrm{FGA}}^{2}}{\pi^{2}\sigma^{4}}-\mathrm{area}_{\mathrm{Inc}}\right), \tag{5}$$

where σ_{D} is the fatigue limit. With eq. (5), sampling-based sensitivity values are calculated with direct Monte-Carlo simulation [33,34]. For the case investigated, the values of the parameters are referred to that of RB180, so that G is 79 GPa, C is 1, l_{m} is 575 nm and σ_{D} is 600 MPa, respectively. Local stress σ, ΔK_{FGA}, and inclusion size $\sqrt{\mathrm{area}_{\mathrm{Inc}}}$ are assumed to be random variables. The stress is normally distributed with a mean value of 750 MPa and a coefficient of variation (COV) of 0.03. ΔK_{FGA} is a normal distribution with a mean value of 5.5 MPa $\mathrm{m}^{1/2}$ and a COV of 0.03. Inclusion size is Gumbel distributed with a mean value of 30 μm and a COV of 0.4.

In this sensitivity analyses, both sensitivity of mean value S_{μ} and sensitivity of standard deviation S_{σ} are dimensionless and appropriate for variable ranking, which are defined as [33]:

$$S_{\mu_{\mathrm{i}}}=\frac{\partial P_{\mathrm{f}}/P_{\mathrm{f}}}{\partial\mu_{\mathrm{i}}/\sigma_{\mathrm{i}}},\quad S_{\sigma_{\mathrm{i}}}=\frac{\partial P_{\mathrm{f}}/P_{\mathrm{f}}}{\partial\sigma_{\mathrm{i}}/\sigma_{\mathrm{i}}}, \tag{6}$$

where P_{f}, μ_{i} and σ_{i} are respectively the probability of failure, mean value and standard deviation of a variable X_{i}. The higher the absolute value of S_{μ} or S_{σ}, the more sensitive to fatigue failure for the variable.

Figure 10 shows the fatigue life scattering calculated by Monte-Carlo simulation with eq. (5). The values of fatigue life corresponding to the failure probability of 5%, 50% and 95% are plotted for different stress levels. The mid value of fatigue life increases with the decrease of stress, and the life scattering also increases.

Figure 11 shows the sensitivity evaluation of inclusion size, loading stress and ΔK_{FGA} for the life of VHCF crack initiation. It is seen that fatigue failure is more sensitive to the mean value of stress with regard to S_{μ} (Figure 11(a)) and to the standard deviation of ΔK_{FGA} with regard to S_{σ} (Figure 11(b)). In terms of absolute value of S_{μ}, the influence of mean value for the variables of inclusion size and ΔK_{FGA} is almost the same and the more sensitive variable is loading stress as shown in Figure 11(a). Although inclusion size has an effect on the life scatter by three orders when the loading stress is given for UL150, VHCF failure with FGA has a lower sensitivity of inclusion size under rotating bending with the stress gradient along the radius direction. As shown in Figure 11(b), the standard deviation of stress and inclusion size has a decreasing influence on fatigue

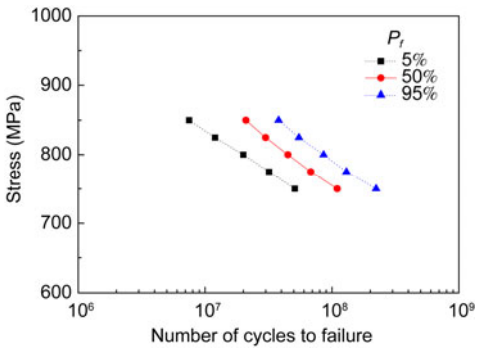

Figure 10 (Color online) Fatigue life scattering by Monte-Carlo simulation.

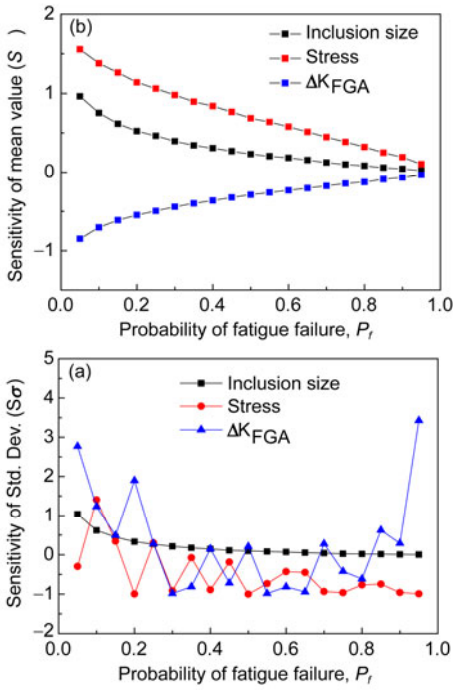

Figure 11 (Color online) (a) sensitivity of mean value, and (b) sensitivity of standard deviation (Std. Dev.).

failure, whereas the standard deviation sensitivity of ΔK_{FGA} is higher than that of stress and inclusion size. For the case of interior inclusion initiation of RB300 and UL150 specimens, the fatigue failure becomes more sensitive to ΔK_{FGA} deviation, resulting in the large life scattering.

6 Conclusions

VHCF tests for specimens of a high carbon chromium steel with three heat treatment procedures were performed with rotating bending and axial cycling conditions. S-N data show an increasing tendency of life scatter for specimens tempered at 300°C. Under rotating bending, interior inclusion initiation is dominant for specimens tempered at 180°C and 300°C, whereas interior grain boundary initiation is dominant for specimens tempered at 150°C. Under axial cycling, inclusion initiation prevails and there is a larger range of size distribution of inclusions as crack origin due to the larger control volume condition. The relationship between inclusion size and fatigue life differs from each other for the two loading conditions. Under rotating bending, local stress, inclusion size and ΔK_{FGA} are essential variables. The sensitivity evaluations show that fatigue failure is more sensitive to the mean values of loading stress, followed by inclusion size and ΔK_{FGA}.

This work was supported by the National Basic Research Program of China (Grant No. 2012CB937500) and the National Natural Science Foundation of China (Grant Nos. 11172304, 11021262 and 11202210).

1 Naito T, Ueda H, Kikuchi M. Fatigue behavior of carburized steel with internal oxides and nonmartensitic microstructure near the surface. Metall Trans A, 1984, 15(7): 1431–1436
2 Sakai T, Lian B, Takeda M, et al. Statistical duplex S-N characteristics of high carbon chromium bearing steel in rotating bending in very high cycle regime. Int J Fatigue, 2010, 32(3): 497–504
3 Murakami Y, Yokoyama N N, Nagata J. Mechanism of fatigue failure in ultralong life regime. Fatigue Fract Eng Mater Struct, 2002, 25(8-9): 735–746
4 Nakajima M, Tokaji K, Itoga H, et al. Effect of loading condition on very high cycle fatigue behavior in a high strength steel. Int J Fatigue, 2010, 32(2): 475–480
5 Zhao A G, Xie J J, Sun C Q, et al. Effects of strength level and loading frequency on very-high-cycle fatigue behavior for a bearing steel. Int J Fatigue, 2012, 38: 46–56
6 Zhang Y Y, Duan Z, Shi H J. Comparison of the very high cycle fatigue behaviors of INCONEL 718 with different loading frequencies. Sci China-Phys Mech Astron, 2013, 56(3): 617–623
7 Tschegg E, Stanzl S. Fatigue crack propagation and threshold in b.c.c. and f.c.c. metals at 77 and 293 K. Acta Metall, 1981, 29(1):33–40
8 Duan Z, Shi H, Ma X. Fish-eye shape prediction with gigacycle fatigue failure. Fatigue Fract Eng Mater Struct, 2011, 34(10): 832–837
9 Zimmermann M. Diversity of damage evolution during cyclic loading at very high numbers of cycles. Int Mater Rev, 2012, 57(2): 73–91
10 Sakai T. Review and prospects for current studies on very high cycle fatigue of metallic materials for machine structural use. J Solid Mech Mater Eng, 2007, 3(3): 425–439
11 Grad P, Reuscher B, Brodyanski A, et al. Mechanism of fatigue crack initiation and propagation in the very high cycle fatigue regime of high-strength steels. Scripta Mater, 2012, 67(10): 838–841
12 Lai J, Lund T, Rydén K, et al. The fatigue limit of bearing steels – Part I: A pragmatic approach to predict very high cycle fatigue strength. Int J Fatigue, 2012, 38(0): 155–168
13 Stepanskiy L G. Cumulative model of very high cycle fatigue. Fatigue Fract Eng Mater Struct, 2012, 35(6): 513–522
14 Hong Y S, Lei Z Q, Sun C Q, et al. Propensities of crack interior initiation and early growth for very-high-cycle fatigue of high strength steels. Int J Fatigue, 2014, 58: 144–151
15 Wang Q Y, Bathias C, Kawagoishi N, et al. Effect of inclusion on subsurface crack initiation and gigacycle fatigue strength. Int J Fatigue, 2002, 24(12): 1269–1274
16 McDowell D L, Dunne F P E. Microstructure-sensitive computational modeling of fatigue crack formation. Int J Fatigue, 2010, 32(9): 1521–1542
17 Shiozawa K, Morii Y, Nishino S, et al. Subsurface crack initiation and propagation mechanism in high-strength steel in a very high cycle fatigue regime. Int J Fatigue, 2006, 28(11): 1521–1532
18 Murakami Y, Nomoto T, Ueda T, et al. On the mechanism of fatigue failure in the superlong life regime (N > 10(7) cycles). Part I: influence of hydrogen trapped by inclusions. Fatigue Fract Eng Mater Struct, 2000, 23(11): 893–902
19 Liu Y B, Yang Z G, Li Y D, et al. Dependence of fatigue strength on inclusion size for high-strength steels in very high cycle fatigue regime. Mater Sci Eng A, 2009, 517(1-2): 180–184
20 Li S X. Effects of inclusions on very high cycle fatigue properties of high strength steels. Int Mater Rev, 2012, 57(2): 92–114
21 Zhao A G, Xie J J, Sun C Q, et al. Prediction of threshold value for FGA formation. Mater Sci Eng A, 2011, 528(22-23): 6872–6877
22 Lei Z Q, Hong Y S, Xie J J, et al. Effects of inclusion size and location on very-high-cycle fatigue behavior for high strength steels. Mater Sci Eng A, 2012, 558: 234–241
23 Ritchie R O, Chang V A, Paton N E. Influence of Retained Austenite

on Fatigue Crack-Propagation in Hp9-4-20 High-Strength Alloy-Steel. Fatigue Eng Mater, 1979, 1(1): 107–121
24 Wei D Y, Gu J L, Fang H S, et al. Fatigue behavior of 1500 MPa bainite/martensite duplex-phase high strength steel. Int J Fatigue, 2004, 26(4): 437–442
25 Lee C S, Lee K A, Li D M, et al. Microstructural influence on fatigue properties of a high-strength spring steel. Mater Sci Eng A, 1998, 241(1-2): 30–37
26 Murakami Y, Endo M. Effects of defects, inclusions and inhomogeneities on fatigue-strength. Int J Fatigue, 1994, 16(3): 163–182
27 Yang Z G, Zhang J M, Li S X, et al. On the critical inclusion size of high strength steels under ultra-high cycle fatigue. Mat Sci Eng A, 2006, 427(1-2): 167–174
28 Sun C Q, Lei Z Q, Xie J J, et al. Effects of inclusion size and stress ratio on fatigue strength for high-strength steels with fish-eye mode failure. Int J Fatigue, 2013, 48: 19–27
29 Sun C Q, Xie J J, Zhao A G, et al. A cumulative damage model for fatigue life estimation of high-strength steels in high-cycle and very-high-cycle fatigue regimes. Fatigue Fract Eng Mater Struct, 2012, 35(7): 638–647
30 Tanaka K. A theory of fatigue crack initiation at inclusions. Metall Trans A, 1982, 13(1): 117–123
31 Baldissera P, Delprete C. The formal analogy between Tanaka-Mura and Weibull models for high-cycle fatigue. Fatigue Fract Eng Mater Struct, 2012, 35(2): 114–121
32 Lei Z Q, Zhao A G, Xie J J, et al. Very high cycle fatigue for GCr15 steel with smooth and hole-defect specimens. Theore Appl Mech lett, 2012, 2: 031003
33 Wu Y T, Mohanty S. Variable screening and ranking using sampling-based sensitivity measures. Reliab Eng Sys Safety, 2006, 91(6): 634–647
34 Lei Z Q, Xie J J, Zhao A G, et al. A simulation on microstructure sensitivity to very-high-cycle fatigue behavior of metallic materials. Procedia Eng, 2010, 4: 225–232